trapped beam (vertical orientation), since this maximizes the overlap of the cell volume with the region of highest light field. As the size of the bright annulus increases with mode order, maximum overlap between the cell volume and the trapping field is expected for cell orientation away from the vertical direction. For l =10 the cell can be seen to be oriented in the horizontal plane that is the trapping plane as this maximizes the overlap of the cell volume with the region of highest light field.

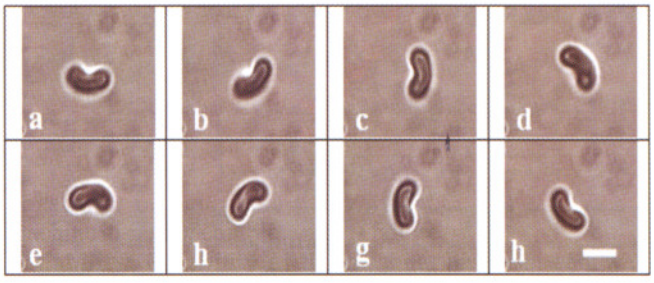

Fig. L.6.2. The rotation of a trapped RBC via transfer of light orbital angular momentum when trapped under l=15 mode. In (a)-(h) the cell is observed to be rotated by an angle of 45° over the previous frame. The time separation between the frames is ~ 625 ms. Scale bar, 5 μm.

We also observed that the torque exerted by LG trapping beam with high topological charges (|l|~ 15 or more) could drive RBCs as natural micro-rotors. For |l| ~ 15 the trapped cells get aligned over the bright annulas of the LG trap due to larger circumference of the annulas. Under such condition the cells while being contained within the annular ring of light, orbits the beam axis in a direction determined by the handedness of the helical phase fronts. This is believed to be due to the transfer of light orbital angular momentum to the trapped cells by the scattering of the trap beam having helical wavefront. Fig. L.6.2 shows the rotation of an RBC when trapped under l = 15 mode. The observed rotational frequency was ~ 12 rpm at ~ 15 mW of trapping power and it can be increased using higher trap beam power. To check whether the observed rotation is caused by the transferred light orbital angular momentum from the trap beam to the cell we changed the helicity of the trap beam. The sense of rotation was observed to get reversed as the charge of the LG mode was made negative. This allows for a means to change the sense of rotation of a micro-rotor system by simply changing the helicity of the trapping beam. Such control over rotational sense is not possible with techniques utilizing specially fabricated micro-structures or RBCs suspended in hypertonic buffers. A control on the sense of rotation can facilitate bi-directional operation for micro-machine components like micro-motors or valves.

Reported by:
R. Dasgupta (raktim@rrcat.gov.in), S. Ahlawat, R. S. Verma and P. K. Gupta

L.7: 5 kW CW CO_2 Laser for Material Processing

A 5 kW CW CO_2 laser system was developed long back in LMPD. With time, various problems concerned in performance of high power CW CO_2 laser viz. rapid decrease in beam shape & size and laser power, short gas lifetime, electrode deposits, fast degradation of cavity mirrors and frequent replacement/maintenance of laser sub-systems were recorded. Therefore, the existing 5 CW CO_2 laser system has been renovated to overcome these problems and improve its performance. Various modifications in design of laser sub-systems have been done. All the mechanical sub-systems, except vacuum chamber, vacuum pump and SMPS; were redesigned, procured and assembled. The major modified components of laser system are various subassemblies viz blowers, gas flow loop, electrodes, resonator, coolant circuit etc. Some of the important modifications made in the laser system (Fig.L.7.1) are described below.

Fig.L.7.1: Renovated 5kW CW CO_2 laser

Corrosion of blower housing, motors, ducts and supporting structure have been minimized through suitable choice of materials.

Belt drive of blower is replaced with direct drive to eliminate debris from belt and pulley drive.

In the electrode assembly, epoxy, araldite and PVC tubing are replaced with high temperature materials to minimize degradation from discharge-induced UV radiation.

All four cavity mirrors are mounted on a single resonator structure to minimize cavity misalignment.

A secondary coolant circuit (Fig. L.7.2A) has been introduced to eliminate contamination from other laser systems.

A gas purging system, consisting of purging controller (Fig.L.7.2B), gas cylinder bank and gas changeover, has been introduced for long-term laser operation.

- Flow monitor-cum-switches have been introduced for safety interlocking to prevent accidental switching on of laser system without coolant.
- A pneumatically operated beam shutter-cum-beam dump has been added.

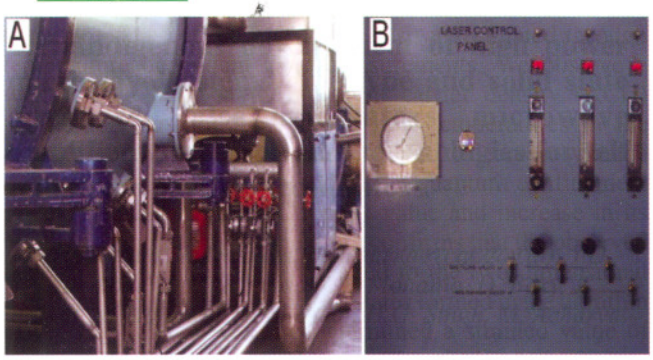

Fig.L.2.2: (A) Secondary coolant circuit and (B) gas purging controller.

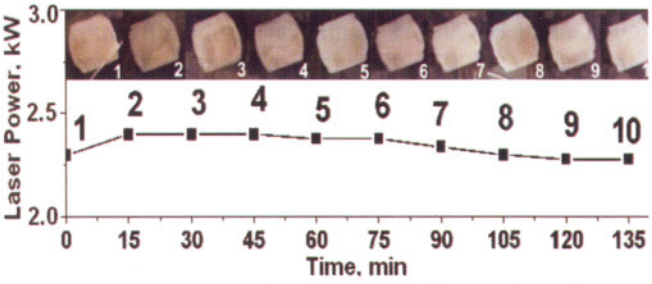

Fig.L.7.3: Variation of laser power & beam shape during laser operation in single filling/isolation mode.

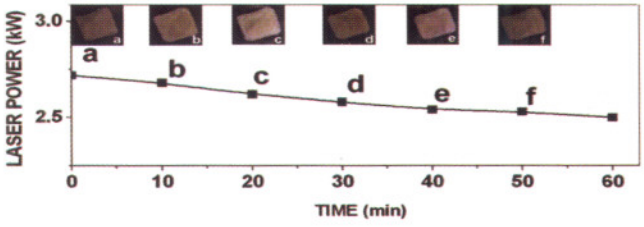

Fig.L.7.4: Variation of laser power and beam shape during laser operation in purging mode.

The performance of renovated laser system has been tested. The transparent glow discharge was achieved and a total 63 kW input power was dissipated in 2 x 1 m long discharge zone with inter electrode gap of 35 mm. The optimum gas mixture was: 2 mbar of CO_2, 14 mbar of N_2 and 34 mbar of He. Laser system delivered maximum output power of 5.8 kW with electro-optic efficiency of 14%. Figs. L.7.3 and L.7.4 present variation of output laser power and beam shape and size during laser operation in single filling/isolation and optimized purging modes, respectively. The maximum variation in laser power during 135 min. long laser operation in purging mode was about ± 3%. The shape and size of laser beam remained almost unchanged during the operation of the laser system.

Reported by:
Harish Kumar (harishk@rrcat.gov.in)

L.8: Effect of volume fraction on the third-and fifth-order nonlinearity of nanoplatelet colloids

Transient absorption measurements can be used to study the carrier dynamics as well as the nonlinearity of a material. Using this technique, we have measured the effect of volume fraction of silver in water, on the imaginary part of third- and fifth-order nonlinearities in silver nanoplatelet colloid.

The optical response of a colloidal material formed by dilutely dispersed metal nanoparticles in a host depends on the dielectric constants of the host as well as the nanoparticle. When the nonlinear response of the material is instantaneous, a generalized Maxwell-Garnett theory with T-matrix formalism can be used to understand its various nonlinear susceptibilities. Experimental measurement on scaling of the nonlinear optical coefficients with the volume fraction is used to validate the theoretical results. However, for materials with slow response there are no experimental and theoretical investigations. In metal the hot electron contribution to the nonlinearity is slow since it takes about 350 fs for the electrons to thermalize. Our measurements were performed using a 100 fs pulses delivered by a Ti:Sapphire laser operated at 800 nm wavelength. Thus the pulse width used in the experiment was lower than the thermaization time of electrons. The silver nanoplatelets colloid studied has localized surface plasmon resonance (LSPR) at 787 nm and 331 nm.

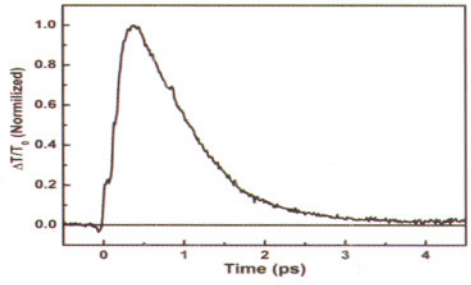

Fig. L.8.1. The time dependent transimitivity of silver nanoplatelets in water near in-plane dipole resonance.

Fig. L.8.1 shows a typical transient response of the metal nanoparticle in water. The transmission (T) of the sample increases with the arrival of the pump pulse and peaks at around 370 fs delay between pump and probe. In subsequent time the transimitivity of the colloid reduces. The peak change in the absorption of the sample was estimated from the peak change in transimitivity. Fig. L.8.2 shows the intensity dependence of the peak change in the absorption of the sample for various volume fractions of silver in water. The increases with the increase in intensity of the pump pulse. However, at higher intensities tend to saturate showing the effect of fifth-order nonlinearity. Further, with increase in volume fraction of silver the change in absorption of the sample increases.